Pre-steady-state kinetic and mutational insights into mechanisms of endo- and exonuclease DNA processing by mutant forms of human AP endonuclease

Artemiy Bakman, Alexander Ishchenko, Murat Saparbaev, Olga Fedorova, Nikita Kuznetsov

Pre-steady-state kinetic and mutational insights into mechanisms of endo- and exonuclease DNA processing by mutant forms of human AP endonuclease*

Artemiy S. Bakman[1], Alexander A. Ishchenko[2], Murat Saparbaev[2], Olga S. Fedorova[1], Nikita A. Kuznetsov[1,3§]

[1]Institute of Chemical Biology and Fundamental Medicine, Siberian Branch of Russian Academy of Sciences, Novosibirsk 630090, Russia
[2]Group «Mechanisms of DNA Repair and Carcinogenesis», Equipe Labellisée LIGUE 2016, CNRS UMR9019, Université Paris-Saclay, Gustave Roussy Cancer Campus, F-94805 Villejuif Cedex, France.
[3]Department of Natural Sciences, Novosibirsk State University, Novosibirsk 630090, Russia

*Running title: *Kinetics of substrate recognition by APE1 mutants*

[§]To whom correspondence should be addressed: N.A.K. Tel: +7 (383) 363-5174, Email: Nikita.Kuznetsov@niboch.nsc.ru

Keywords: DNA repair, apurinic/apyrimidinic endonuclease, DNA-protein interaction, conformational change, substrate recognition, active site, fluorescence, pre-steady-state kinetics.

Abbreviations: AP site, apurinic/apyrimidinic site; F, (2R,3S)-2-(hydroxymethyl)-3-hydroxytetrahydrofuran; DHU, 5,6-dihydrouridine; αA, α-adenosine; BER, base excision repair; NIR, nucleotide incision repair; FRET, Förster resonance energy transfer; PAGE, polyacrylamide gel electrophoresis

ABSTRACT

Human apurinic/apyrimidinic endonuclease APE1 catalyzes endonucleolytic hydrolysis of phosphodiester bonds on the 5′ side of structurally unrelated damaged nucleotides in DNA or native nucleotides in RNA. APE1 additionally possesses 3′-5′-exonuclease, 3′-phosphodiesterase, and 3′-phosphatase activities. According to structural data, endo- and exonucleolytic cleavage of DNA is executed in different complexes when the excised residue is everted from the duplex or placed within the intrahelical DNA cavity without nucleotide flipping. The interaction between residues Arg177 and Met270, which was hypothesized recently to be a switch for endo- and exonucleolytic catalytic mode regulation, was verified by pre–steady-state kinetic analysis of the R177A APE1 mutant. The function of another DNA-binding–site residue, Arg181, was analyzed too; it changed its conformation when enzyme–substrate and enzyme–product complexes were compared. Mutation R181A significantly facilitated the product dissociation stage and only weakly affected DNA-binding affinity. Moreover, R181A reduced the catalytic rate constant severalfold due to a loss of contact with a phosphate group. Finally, the protonation/deprotonation state of residues Tyr171 and His309 in the catalytic reaction was verified by their substitution. Mutations Y171F and H309A inhibited the chemical step of the AP endonucleolytic reaction by several orders of magnitude with retention of capacity for (2*R*,3*S*)-2-(hydroxymethyl)-3-hydroxytetrahydrofuran-containing-DNA binding and without changes in the pH dependence profile of AP endonuclease activity, indicating that deprotonation of these residues is likely not important for the catalytic reaction.

INTRODUCTION

Human apurinic/apyrimidinic endonuclease 1 (APE1) is a multifunctional protein that is required for cell viability (1–8). This enzyme recognizes apurinic/apyrimidinic (AP) sites in DNA and cleaves the 2′-deoxyribose-phosphate backbone of DNA 5′ to an AP site to generate 3′-hydroxyl and 5′-deoxyribose phosphate (dRP) groups at the DNA ends (AP endonuclease activity) (9). Nonetheless, APE1 has been found to recognize and process as substrates some damaged nucleosides too (nucleotide incision repair [NIR] activity), for example, 5,6-dihydro-2′-deoxyuridine (DHU), alpha-2′-deoxyadenosine (αA) (10), and 2′-deoxyuridine (U) (11). In addition, APE1 has 3′-5′-exonuclease activity (12–14) as well as 3′-phosphodiesterase, 3′-phosphatase (15), and endoribonuclease (16–20) activities.

APE1 activities toward a wide range of its substrates are realized by the same active site that is formed by residues Asp308, His309, Glu96, Asp70, Asp210, Tyr171, Asn212, and Asn174 as revealed by crystal structures of enzyme–substrate complexes (21–23). For APE1 catalysis, a Mg^{2+} ion is required as a cofactor. This ion is coordinated by residues Glu96 and Asp70 and water molecules in the active site (24–26). The DNA binding involves residues Arg73, Ala74, Lys78, Arg156, Arg181, Trp280, Asn222, Asn226, and Asn229, which come into contact with phosphate groups of the DNA duplex on 5′ and 3′ sides of the AP-site. Residues Tyr128 and Thr268 span and widen the minor groove of DNA by ~2 Å. The everted damaged nucleotide is placed into the enzyme's binding pocket, which is formed by Asn174, Asn212, Asn229, Ala230, Phe266, and Trp280. Into the space (in the DNA helix) freed by the everted damaged nucleotide, two amino acid residues (Arg177 and Met270) are inserted, which form molecular tweezers that strongly constrain DNA (27).

Although the mechanism of the APE1 AP-endonuclease activity has been quite extensively studied to date (28–31), the roles of some APE1's active-site amino acid residues are debated in the literature. Thus, according to the catalytic mechanism based on the crystal structure data (**Fig. 1, A**), residues Tyr171 and His309 should be protonated to stabilize the DNA phosphate group in the transition state complex (**Fig. 1, B**) (21, 22). Nonetheless, some experimental data suggest that Tyr171 and/or His309 may participate in the cleavage reaction in the deprotonated form (32, 33). On the other hand, when deprotonated, these amino acid residues can activate a nucleophilic water molecule rather than coordinate the negatively charged scissile phosphate as suggested in alternative mechanisms (34, 35) (**Fig. 1, C**). Recently, it was suggested (33) that the ionized state of these residues is a molecular switch between the alternative catalytic mechanisms, which involve different functionalities of these residues throughout the reaction.

Another question of great interest is how a single APE1 active site can process a wide range of substrates (23, 28, 36–38). Research on the APE1 3′-5′-exonuclease activity has suggested that the hydrophobic pocket comprised of Phe266 and Trp280 restricts enzyme substrate specificity (23). It should be noted that DNA structural features of APE1 exerting 3′-5′-exonuclease activity have been revealed to contrast sharply with those during an AP endonuclease reaction.

In fact, an AP-site is flipped out from a DNA helix into the protein active site. By contrast, in the case of APE1 3′-5′-exonuclease activity, the excised nucleotide is placed within the intrahelical DNA cavity without nucleotide flipping (**Fig. 2**) (23). Currently, there are no crystal structures of APE1 complexes with damaged-base–containing DNA; therefore, the mechanism of NIR activity remains unclear. Based on the structures of complexes of APE1 with DNA (23), it has been suggested that during cleavage of NIR substrates, APE1 uses an exo-like intrahelical mechanism for the reason that these substrates are bulky and would require considerable active-site pocket volume. Besides, the optimal conditions for NIR activity are very similar to those required for the APE1 exonuclease activity and differ from those for the AP-endonuclease activity (10). Nevertheless, a molecular dynamics study of APE1 NIR-activity in conjunction with pulsed electron–electron double resonance (PELDOR) spectroscopy and pre–steady-state kinetic analysis suggests that damaged nucleotides are flipped out from the DNA helix into APE1's binding pocket (28).

A recently published report revealed that the interaction between APE1 and its AP-endo- and exo-DNA-substrates induces a conformational change of residue Arg177 resulting in the interaction between Arg177 and Met270 ("RM bridge") (36). This "RM bridge" has been supposed to perform a key function in exonuclease activity and to give APE1 the AP-site specificity (36). By contrast, our previous analysis of M270A APE1 activity has not revealed significant changes in APE1 substrate specificity in comparison with wild-type (WT) APE1 (30). Hence, the meaning of the "RM bridge" for APE1 specificity requires additional research.

Stopped-flow experiments with Trp fluorescence detection in WT APE1 have been conducted previously, and the kinetic mechanism of protein conformational changes has been determined (39–41). Because of one of seven Trp residues of APE1 (Trp280) is located in the DNA-binding pocket of the enzyme and forms a hydrogen bond with the 3′ phosphate group of the AP-site, the observed changes in Trp fluorescence most likely reflect the conformational changes near the Trp280 residue. However, Trp267 residue is also located in the vicinity of a hydrophobic pocket of the active site and could be responsible for changes in the fluorescent signal of APE1.

Changes in Trp fluorescence intensity allow us to identify the steps of DNA binding, cleavage, and a product release. It is worth noting that the enzyme–substrate binding proceeds in two steps as evidenced by monitoring of 2-aminopurine (42), Trp (39), and carboxyfluorescein (FAM) (43)

fluorescence traces. The first step is the formation of the primary enzyme–substrate complex may include an interaction between the phosphate groups of the DNA duplex on the 5′ and 3′ sides of an F-site [(2*R*,3*S*)-2-(hydroxymethyl)-3-hydroxytetrahydrofuran] and amino acid residues of the substrate-binding cleft. This step is associated with desolvation of polar groups in the protein–DNA contact area and a release of highly ordered crystalline water molecules from DNA grooves (44). It seems that at this moment, the insertion of Arg177 and Met270 takes place, which is accompanied by displacement of crystalline water from DNA grooves. At the second step of the interaction of APE1 with an F-substrate (F-site–containing DNA), a specific rearrangement of the primary complex occurs, which includes eversion of the F-site into the enzyme active site. Then, the catalytic stage of the process takes place and causes the formation of products and subsequent dissociation of the enzyme–product complex; the latter event is accompanied by an increase in Trp fluorescence intensity at later time points.

The above information indicates that detailed investigation of the functions of some APE1 amino acid residues is of great interest because it could help to gain a better insight into the process of APE1 interaction with its substrates. Actually, the aforementioned residues Tyr171, His309, and Arg177 do require clarification of their roles in catalysis. Besides, here, we decided to elucidate the functions of the Arg181 residue because it has been reported to change its conformation during the enzyme–DNA interaction, and this change may affect substrate binding or product dissociation steps (22).

Therefore, the aim of this study was to clarify the roles of residues Tyr171, His309, Arg177, and Arg181 (**Fig. 3**) in the interaction between APE1 and DNA. For this purpose, APE1 mutants with substitutions Y171F, H309A, R177A, and R181A were obtained. The interaction between these APE1 mutants and DNA containing a synthetic analog of an AP-site was investigated by the stopped-flow fluorescence method, which allows to monitor the conformational changes in APE1 and DNA during their interaction. Activity of the APE1 mutants toward different DNA substrates (AP-endo-, exo-, and NIR substrates) was also studied by direct detection of the product formation by polyacrylamide gel electrophoresis (PAGE). Additionally, the impact of pH on the AP-endonuclease activity of Y171F and H309A APE1 was investigated to test the hypothesis that these residues take part in the catalytic reaction in the deprotonated state.

EXPERIMENTAL PROCEDURES

Site-directed mutagenesis and protein purification

Mutations Y171F, R177A, R181A, and H309A were introduced into the pET11a-APE1 plasmid using a site-directed mutagenesis kit (QuikChange XL, Stratagene). For expression of the recombinant proteins, 1 L culture of *Escherichia coli* strain Rosetta II(DE3) (Invitrogen, France) (in 2xYT broth) carrying the pET11a-APE1 construct was grown at 100 μg/mL ampicillin and 25 μg/mL chloramphenicol and 37°C until absorbance at 600 nm (A_{600}) reached 0.6–0.7. APE1 expression was induced overnight with 0.5 mM isopropyl-β-D-thiogalactopyranoside at 25°C. In the case of the H309A APE1 mutant, to increase the yield of the protein, the APE1 induction was carried out in *E. coli* strain Arctic Express at 15°C. Isolation and purification of the enzymes were performed as described earlier (44, 45). The protein concentration was measured by means of A_{280}; stock solutions were stored at −20°C in 50% glycerol.

DNA substrates

Sequences of the DNA and RNA substrates employed in this work are presented in Table 1. Oligodeoxynucleotides (ODNs) were synthesized by standard phosphoramidite methods on an ASM-800 synthesizer (BIOSSET Ltd., Novosibirsk, Russia) using phosphoramidites purchased from either Glen Research or ChemGenes. The synthetic ODNs were purified by HPLC on an Agilent 1200 chromatograph (USA) and a Zorbax SB-C18 column (5 μm, 4.6 × 150 mm) via a linear gradient of acetonitrile (0 → 50%) in the presence of 20 mM triethylammonium acetate (pH 7.0) for 30 min at a flow rate of 2 mL/min. Fractions containing ODNs were dried in vacuum, dissolved in water, and precipitated with 2% $LiClO_4$ in acetone. After washing with pure acetone and drying, the ODN precipitates were dissolved in water and stored at −20°C until experiments. Concentrations of the ODNs were determined by means of A_{260}. Homogeneity of the purified ODNs was evaluated by PAGE in a denaturing 20% gel. The ODNs were visualized with the Stains-All dye (Sigma, USA). All DNA duplexes were prepared by annealing of modified and complementary strands at the 1:1 molar ratio in an aqueous solution.

It could be noted that the DNA substrates that are referred to as F/G, FAM-F/G and FRET-F/G differ only in dye labels at the duplex ends; F-site has been used as an AP site analogue. The substrate F/G has no any dyes, because we used it for kinetic assays with detection of intrinsic fluorescence of the enzyme's Trp residues. For the PAGE analysis of the DNA cleavage we used the

substrate FAM-F/G. The fluorescent label at 5' end of F-site containing chain allowed us to visualize cleaved and non-cleaved DNA after the separation in the polyacrylamide gel. For FRET fluorescence assays we used the substrate FRET-F/G which carries fluorescence emitter FAM and quencher BHQ1 at the opposite ends of DNA duplex. This substrate allowed us to monitor the changes in the distance between duplex ends by detecting the FAM fluorescence intensity.

PAGE analysis of the DNA cleavage

A FAM-F/G-substrate was subjected to cleavage analysis by PAGE in experiments on a comparison of APE1 mutants' activities, in analyses of kinetic time courses for Y171F and H309A APE1 mutants and in an assay for the impact of pH on the activities of these two APE1 mutants.

To start a reaction between an enzyme and substrate, their solutions were mixed in reaction buffer consisting of 50 mM HEPES-KOH pH 6.8, 50 mM KCl, 6 mM $MgCl_2$, 1 mM EDTA, 1 mM DTT, and 7% of glycerol (v/v) unless stated otherwise.

In addition, FAM-DHU/G and FAM-αA/T substrates (NIR activity assays) and the Exo-substrate (exonuclease activity assay) were subjected to cleavage analysis by PAGE.

NIR activity assays for DHU/G- and αA/T-substrates were performed at 25°C in NIR buffer composed of 20 mM NaH_2PO_4/Na_2HPO_4 pH 6.8, 50 mM KCl, 0.1 mM $MgCl_2$ 1 mM DTT, and 7% of glycerol (v/v).

The exonuclease activity assay was performed at 37°C in a buffer consisting of 50 mM Tris-HCl pH 7.5, 50 mM KCl, 6 mM $MgCl_2$ 1 mM EDTA, 1 mM DTT, and 7% of glycerol (v/v).

Concentrations of reactants and reaction times for NIR activity and exonuclease activity assays are given in Table 2. Typically, data obtained by PAGE analysis were averaged as results of at least three replicates.

pH dependence assay

In the pH dependence assay, reaction buffers contained the same components at the same concentrations, except that instead HEPES-KOH they contained NaH_2PO_4/Na_2HPO_4 for pH 6.0 and 6.5 or Tris-HCl for pH 7.0, 7.5, 8.0, 8.5, and 9.0.

In all cases, the reaction was conducted at 25°C, and at a certain time point, the reaction was immediately quenched with a gel-loading dye containing 8 M urea and 25 mM EDTA. The obtained samples were desalted on hand-made spin-down columns filled with Sephadex G25 (Amersham Biosciences) equilibrated in 8 M urea and then were loaded on a 20% (w/v) polyacrylamide/7 M urea gel. The gels were visualized using an E-Box CX.5 TS gel-documenting system (Vilber Lourman, France) and quantified in the Gel-Pro Analyzer software (Media Cybernetics, Rockville, MD). Relative error of the PAGE method did not exceed 10%. The analysis of pH dependence carried out for mutant forms were performed exactly in the same experimental conditions as described in (33).

In the case of kinetic time courses for Y171F and H309A (single turnover assays), the proportion of the product was fitted to a single exponential curve using the Origin software (Originlab Corp.):

$$[\text{product}] = A \times [1 - \exp(-k^{PAGE}t)] \quad (1)$$

where A is amplitude, k^{PAGE} is the rate constant, and t is reaction time.

To analyze the dependences of the enzymatic activity on pH we assumed that enzyme is characterized by acidity constant K_a, i.e., the thermodynamic constant corresponding to the enzyme deprotonation process. This constant could characterize the total acidity constants of some amino acid residues affecting the enzymatic activity (**Scheme 1**).

Scheme 1. Enzyme deprotonation process.

$$EH^+ \overset{K_a}{\rightleftharpoons} E + H^+,$$

where E denotes the deprotonated enzyme's molecule, EH^+ is the protonated enzyme's molecule.

The thermodynamic constant of this process corresponds to equation (2):

$$K_a = \frac{[E][H^+]}{[EH^+]} \quad (2)$$

The sum of protonated and deprotonated enzyme concentrations is equal a total concentration of the enzyme ($[E]_t$):

$$[E]_t = [E] + [EH^+] \quad (3)$$

Hence, the fraction of the deprotonated enzyme (α_E) depends on pH according to following equation:

$$\alpha_E = \frac{[E]}{[E]_t} = \frac{1}{1+\frac{[H^+]}{K_a}} = \frac{1}{1+10^{(pKa-pH)}} \quad (4)$$

Herewith, the fraction of the protonated enzyme equals to:

$$\alpha_{EH+} = 1 - \alpha_E \quad (5)$$

If A_{EH+} is the activity of the protonated form of the enzyme and A_E is the activity of the deprotonated form of the enzyme, the observed enzyme's activity A_{obs} would be equal (6):

$$A_{obs} = A_E\alpha_E + A_{EH+}\alpha_{EH+} = A_{EH+} + \left(\frac{A_E - A_{EH+}}{1+10^{(pKa-pH)}}\right) \quad (6)$$

Therefore, the dependence of the enzymatic activity on pH for mutants Y171F and H309A were fitted to this equation.

Stopped-flow fluorescence measurements

Stopped-flow measurements with fluorescence detection were carried out mostly as described previously (46–48) by means of a model SX.20 stopped-flow spectrometer (Applied Photophysics Ltd., UK). The fluorescence of Trp was excited at λ_{ex} = 290 nm and monitored at λ_{em} > 320 nm as transmitted by the WG-320 filter (Schott, Mainz, Germany). If a 6-FAM residue was present in the ODN, then wavelength λ_{ex} = 494 nm was utilized to excite this residue, and its emission was analyzed at λ_{em} > 530 nm (Schott filter OG-530).

The concentration of the enzyme in all the experiments with Trp fluorescence detection was 1.0 μM, and the concentration of the F/G-substrate was varied from 0.5 to 3.0 μM. The concentration of the FRET-F/G-substrate in the experiments with FAM fluorescence detection was 1.0 μM, and the enzyme concentration was varied from 0.5 to 3.0 μM. Typically, each trace shown is the average of three or more individual experiments. All the experiments were conducted at 25°C in a buffer consisting of 50 mM HEPES-KOH pH 6.8, 50 mM KCl, 1.0 mM EDTA, 1.0 mM DTT, 6.0 mM $MgCl_2$, and 7% of glycerol (v/v).

Global fitting of stopped-flow data

The sets of kinetic curves obtained at different concentrations of the reactants were analyzed in the DynaFit software (BioKin, Pullman, WA) (49) as described previously (50–53).

This approach is based on fluorescence intensity variation in the course of the reaction owing to sequential formation and subsequent transformation of the DNA–enzyme complex and its conformers. Concentrations of each species in the mechanisms are described by a set of differential equations according to Schemes 2 and 3 (see Results). The stopped-flow fluorescence traces were directly fitted to the fluorescence intensity at any reaction time point as the sum of background fluorescence and fluorescence intensity values of each intermediate complex formed by the enzyme with DNA:

$$F = F_0 + \sum_{i=0}^{n} f_i \times [ES]_i \quad (7)$$

where F_0 is an equipment-related photomultiplier parameter ("noise"), f_i is the molar response coefficient of the ith intermediate ES_i ($i = 0$ corresponds to the free protein in the case of Trp fluorescence detection or the free substrate in the case of FAM fluorescence detection, and $i > 0$ to the enzyme–DNA complexes).

The software performs numerical integration of a system of ordinary differential equations with subsequent nonlinear least-squares regression analysis. In the fits, we optimized all relevant rate constants for the forward and reverse steps as well as specific molar response factors for all intermediate complexes.

To estimate confidence intervals for the rate constants, the Monte–Carlo method (54) was used in DynaFit as described in the DynaFit Scripting manual.

RESULTS

Relative F-site cleavage activities of APE1 mutants as revealed by PAGE

To compare effects of mutations on AP-endonuclease enzymatic activity, we carried out direct PAGE analysis of product accumulation for WT, Y171F, R177A, R181A, and H309A APE1 (**Fig. 4**). In this experiment, AP-endonuclease activity was not detectable in Y171F and H309A mutants, indicating that these amino acid substitutions strongly reduce enzyme catalytic activity. This finding is consistent with literature data (32, 55–58). In the case of R181A, AP-endonuclease activity diminished only slightly, and R177A APE1 was found to be ~1.7-fold more active than the WT enzyme consistently with previous data on R177A (21). These differences in F-site cleavage activity detected by steady-state product accumulation analysis may be caused by effects of mutations on enzyme–DNA binding, on the catalytic step, or product dissociation. To clarify the impact of these amino acid substitutions on individual steps of the catalytic mechanism, further experiments were performed.

Single-turnover kinetic time courses of product accumulation

F-site cleavage activity of the least active APE1 mutants, Y171F and H309A, was assessed via single-turnover kinetic time courses of product accumulation (**Fig. 5**). The values of k_{cat} for Y171A and H309A APE1 have been reported previously (32, 56). Therefore, obtained data are aimed rather to compare the activity of mutant forms at the same concentration conditions. It was found that these mutant forms retain AP-endonuclease activity, but their activity is ~10^3–

10^4-fold less than that of WT APE1. Besides, Y171F is ~6-fold more active than H309A. Obtained data is revealed that changes in the enzyme activity associated with these substitutions are in agreement with the literature data.

The influence of pH on activities of mutants Y171F and H309A

In our previous work (33), we proposed that the impact of pH on APE1 catalytic activity may be explained by deprotonation of the Y171 or H309 residue. Furthermore, these residues have been proposed to activate a nucleophilic water molecule in the catalytic mechanism (32, 34, 35). To elucidate this issue, we evaluated the pH impact on the AP-endonuclease activity of Y171F and H309A APE1 mutants.

In the pH range from 6.0 to 9.0 the enzyme activity dependence on pH is consistent with equation (6), therefore supporting that deprotonation of some amino acid residue enhances the catalytic efficiency of the enzyme. It could be suggested, that this dependence associated with several residues with close K_a values.

In spite of our previous assumption (33) that deprotonation of H309 or Y171 could enhance the APE1 activity, it was found that the pH dependence profiles of Y171F and H309A mutants (**Fig. 6**) appeared to be almost identical and similar to that of the WT enzyme. Thus, these data did not confirm the supposition that residues Y171 and H309 participate in the endonucleolytic reaction in the deprotonated state. Therefore, the mechanism in which the Asp210 residue activates a nucleophilic water molecule in accordance with an analysis of crystal structures (21, 22) is consistent with our data.

Analysis of Förster resonant energy transfer (FRET) fluorescence traces

To characterize the influence of the mutations on various steps of the catalytic mechanism, pre–steady-state kinetic assays were performed to evaluate conformational changes in the enzyme and substrate in the course of their interaction.

To study conformational dynamics of DNA during the interaction with APE1, we used the FRET-F/G substrate containing the fluorophore/quencher pair FAM/BHQ1 at 5′ termini of the complementary strands (**Fig. 7**). In this FRET system, the fluorescence intensity of FAM depends on FAM–BHQ1 distance, i.e., the distance between the duplex termini.

FRET fluorescence traces for WT APE1 contain an initial phase of a decrease in the fluorescence intensity corresponding to the formation of the enzyme–substrate complex in which DNA is bent and a subsequent increase of fluorescence intensity corresponding to the DNA cleavage and product dissociation. The stopped-flow fluorescence assay with FAM/BHQ1 fluorescence detection has been performed previously on the WT APE1, and a two-step substrate-binding kinetic mechanism has been established (43). Nonetheless, in some cases, the analysis of fluorescent traces cannot separate these two steps of enzyme–DNA binding (30, 33); this problem can be caused by fluorescent system properties or experimental conditions when, for example, the second step proceeds considerably faster than the first one. When the analysis of the fluorescent traces could not separate the two steps of APE1–DNA binding, we analyzed a kinetic scheme that consists of only one stage of enzyme–substrate recognition including both primary binding and a subsequent specific conformational rearrangement.

In the case of Y171F and H309A APE1, FRET fluorescence traces contained only an initial fast decrease phase, suggesting that these mutants retain the capacity for DNA binding and bending, but their catalysis is too slow to be detected by the stopped-flow fluorescence assay because fluorophore bleaching is faster.

The FRET fluorescence traces for R177A and R181A contain both an initial decrease and subsequent growth of fluorescence intensity, suggesting that these mutants retain both DNA bending and sufficiently strong catalytic activities.

Kinetic curves reflecting an interaction of Y171F or H309A APE1 with the FRET-F-substrate were fitted to **Scheme 2** (**Table 3**). The interaction involving WT, R177A, or R181A APE1 was fitted to **Scheme 3** (**Table 3**).

Scheme 2. The kinetic mechanism of APE1 Y171F and H309A binding to the F-site–containing DNA substrates revealed by Trp fluorescence or FRET fluorescence intensity detection.

$$E + S \underset{k_{-1}}{\overset{k_1}{\rightleftharpoons}} E{\bullet}S$$

where E is the enzyme, S is the DNA substrate, E•S is the enzyme–substrate complex; $k_1/k_{-1} = K_S$: the thermodynamic constant of enzyme–substrate association.

Scheme 3. The kinetic mechanism underlying the processing of the F-substrate by WT, R177A, and R181A APE1, as revealed by Trp fluorescence or FRET fluorescence intensity detection.

$$E + S \underset{k_{-1}}{\overset{k_1}{\rightleftarrows}} E{\bullet}S \xrightarrow{k_2} E{\bullet}P \underset{k_{-3}}{\overset{k_3}{\rightleftarrows}} E + P$$

where E represents the enzyme, S is the F-site–containing DNA substrate, P denotes the DNA product, E•S is the enzyme–substrate complex, and E•P stands for the enzyme–product complex; k_3/k_{-3} = K_P: the product dissociation thermodynamic constant. In some cases, we could not determine constants k_3 and k_{-3} separately but could determine their ratio, K_P.

The obtained data indicated that mutations R177A and R181A lead to a 2–3-fold decrease of K_S, and mutations Y171F and H309A cause a 10–20-fold decrease of K_S. Catalytic constant k_2 for R177A is almost unchanged compared to the WT enzyme, and the R181A substitution diminished k_2 ~3-fold. Additionally, K_P is much greater for R181A and R177A than for WT APE1: 5-fold and ~300-fold, respectively. The kinetic constant of product dissociation k_3 is also greater for the mutants. The increase in K_P means that under steady-state conditions, R177A APE1 was more active than the WT enzyme and that R181A, which has a 3-fold lower catalytic constant, was only slightly less active than WT APE1.

It must be noted that substitutions R177A and R181A led to a strong increase in K_P but a relatively weak decrease in K_S. Such phenomena have been observed previously (22, 59) when an increase of K_P more than 500-fold was registered by an electrophoretic mobility shift assay for R177A.

The significant decrease in catalytic constant k_2 for R181A suggests that the previously documented swinging of this residue during the product formation (22) may not only serve as the product-binding contact but also facilitate the catalytic chemical step, probably because Arg181 interaction with a DNA phosphate facilitates the DNA backbone orientation for a more effective cleavage reaction.

The steady-state rate of DNA cleavage by WT, R177A and R181A APE1 was estimated using constants in **Table 3**. It was found that, the estimated steady-state activity of R181A is barely more than that of WT and the difference in their v_i is within the scope of error. However, v_i of R177A APE1 is ~5-fold more than for WT enzyme. Therefore, obtained pre-steady-state data is well correlate with the steady-state experiment presented in the **Fig. 4**, which revealed that R181A is slightly less active than WT, whereas R177A is more active. Although it should be noted that PAGE experiment is quite rough in general this finding is consistent with kinetic parameters derived from pre-steady-state experiments.

Analysis of Trp fluorescence traces

To study protein conformational dynamics during its interaction with DNA containing the F-site, we recorded intrinsic fluorescence of the enzyme's Trp residues (**Fig. 8**). Previously reported stopped-flow experiments with Trp fluorescence detection for WT APE1 (39–41, 43, 44, 60) allow us to identify the steps of DNA binding, cleavage, and a product release.

Indeed, previously reported data for the APE1 interaction with duplexes incorporating the F-site prompted us to conclude that the initial decrease in Trp fluorescence intensity could be attributed to the process of the formation of an enzyme–substrate complex that is responsible for the catalytic hydrolysis of the internucleotide phosphodiester bond. After that the complex dissociates with the concomitant release of the products of the reaction, which results in the increase in fluorescence intensity.

Trp fluorescence traces for Y171F and H309A, as in the case of FRET traces, contained only a decrease in fluorescence intensity corresponding to the enzyme–DNA binding stage. At the same time, Trp fluorescence traces of R177A and R181A, just as WT Trp traces, contain both an initial decrease and subsequent growth phases, indicating that these mutants retain DNA-binding and DNA cleavage activities.

These Trp fluorescence traces were fitted to **Scheme 2** (Y171F and H309A) or **Scheme 3** (WT, R177A, and R181A), to determine kinetic constants for the corresponding mechanisms (**Table 4**).

Overall, the data revealed by Trp fluorescence trace analysis were consistent with the FRET data. All mutations led to a decrease in the forward kinetic constant of DNA binding, k_1, indicating that all these mutations reduce the DNA-binding ability of the enzyme. Nevertheless, DNA-binding affinity K_S was weaker only for R181A and H309A, suggesting that both residues play an important stabilizing role in the enzyme–substrate complex. The R177A substitution did not affect catalytic constant k_2, and R181A APE1 has 4-fold lower k_2. On the other hand, both mutants R177A and R181A have higher product dissociation constant K_P in comparison with WT APE1. Unlike the K_P revealed by the FRET analysis, in this case, the increases in K_P induced by mutations R177A and R181A were not so huge. This result can be explained by the fact that Trp and FRET fluorescence traces detect different stages of the product dissociation process. Indeed, enzyme–

product complex dissociation should be a multistep process that involves protein dissociation from incised DNA and a melting of the DNA product duplex containing the low-melting 5-mer region. Our stopped-flow fluorescence data did not allow us to resolve the relative order of stages in this dissociation process. It could be concluded that the FRET fluorescence traces help to monitor the development of DNA duplex–melting process, whereas the Trp fluorescence traces help to monitor the process of APE1–DNA dissociation. Nonetheless, if the 5-mer region dissociates from the complex of incised DNA with APE1, then Trp fluorescence traces could also help to monitor such a DNA product melting process. For this reason, FRET and Trp fluorescence traces alone are not enough to unveil the detailed step-by-step mechanism of APE1–product complex dissociation in our experimental system.

The NIR activity assay

In spite of numerous studies on WT APE1, the molecular mechanism of damaged nucleotides discrimination is not yet clear. To investigate the impact of mutations R177A and R181A on the NIR activity of APE1, we performed PAGE cleavage experiments on DHU- and αA-containing DNA substrates (**Fig. 9**). Obtained data allow to compare the activity of tested mutant forms in the same experimental conditions to reveal the effect of amino acid substitutions on the minor enzyme activities. It was found that both mutants showed slightly diminished activity toward the DHU-substrate. Activities of R177A and R181A toward the αA-substrate were barely noticeable and 2–3-fold lower as compared to WT APE1. Because of the very low level of APE1 activity toward the NIR substrates, we could not precisely determine the effect of these mutations during NIR activity. Nevertheless, these data revealed that residues Arg177 and Arg181 do not play a crucial part in APE1 specificity to NIR substrates. We did not find that these residues give APE1 the AP-site specificity or contribute considerably to the NIR activity of APE1.

Exonuclease activity assay

To study the influence of substitutions R177A and R181A on exonuclease activity of APE1, the Exo-substrate was subjected to PAGE cleavage analysis (**Fig. 10**). It was found that mutants R177A and R181A have noticeably weaker exonuclease activity relative to WT APE1. It is worth pointing out that a similar reduction in APE1 exonuclease activity has been observed previously for R177A APE1 (61). The finding that R177A catalytic activity is not lower toward F-site–containing DNA but lower toward the Exo-substrate is of interest. We cannot say whether this diminished exonuclease activity is caused by effects on APE1 DNA 3′-terminal binding or on the chemical step. It is also noteworthy that substitutions R177A and M270A have different effects on enzyme exonuclease activity, although these amino acid residues have a common structural function and act cooperatively (36).

Of note, endonuclease cleavage of αA-substrate is accompanied by simultaneous exonuclease degradation of blunt-ended DNA. As it was shown in **Fig. 10** exonuclease activity of tested enzymes toward DNA substrate with 5′ dangling end the decreases of activity was observed in the order WT<M270A<R181A~R177A, which is fully correlate with the intensity of the exonuclease products in **Fig. 9B**. Therefore, in **Fig. 9B** additionally to the bands of NIR activity at the bottom of the gel we have observed the bands of APE1 exonuclease activity toward the blunt end DNA substrate.

DISCUSSION

The Y171F and H309A APE1 mutants have strikingly weaker AP endonuclease activity owing to a decrease in k_{cat} by ~10^3-fold and 10^4-fold for Y171F and H309A, respectively. Meanwhile, these mutants retain the capacity for specific binding to the F-site–containing DNA duplex. Although mutation H309A was found to decrease K_s in agreement with existing data (56), this influence is not critical and much weaker than the k_{cat} reduction.

It has been previously supposed that Tyr171 and/or His309 participate in the catalytic reaction in the deprotonated state acting as a general base to activate a nucleophilic water molecule or attacking a scissile phosphate directly (32–35). Alternatively, Asp210 is thought to activate a nucleophilic water molecule according to high-resolution crystal structure (21, 22). The pH profiles of Y171F and H309A AP endonuclease activity observed here do not have any significant difference from those reported previously (33) determined by means of WT APE1, indicating that deprotonation of residues Tyr171 and His309 is unlikely play a critical role in the catalytic reaction.

The fact that D210N APE1 has much slower activity than that of H309A or Y171F (30, 56) confirms that residue Asp210 performs the main function in the catalytic reaction by acting as a general base activating a nucleophilic water molecule. Moreover, the weaker affinity for the DNA substrate found for H309A is consistent with the notion that His309 takes part in scissile

phosphate coordination. In contrast, substitution D210N has been found to enhance enzyme–substrate affinity (30, 56) thereby corroborating the participation of Asp210 in nucleophilic-water-molecule activation but not in the DNA coordination. Thus, taken together, our data suggest that Tyr171 and His309 coordinate the scissile phosphate and stabilize the pentacoordinate phosphate transition state of the hydrolytic reaction while protonated rather than by activating nucleophilic water while acting as a general base in the deprotonated state.

Our stopped-flow fluorescence assay of WT, R177A, and R181A APE1 AP-endonuclease activities enabled us to monitor the stages of enzyme–DNA binding, product formation, and enzyme–product dissociation. It was crucial for us to extract (from the kinetic data) separate parameters for the hydrolytic reaction (k_2) and for the product dissociation process (K_P, as well as k_3 and k_{-3}) because steady-state k_{cat} is a complex parameter that may be affected by the rate of product dissociation.

Our data have revealed that substitution R177A does not influence catalytic rate constant k_2 but significantly facilitates enzyme–product dissociation, thus confirming a previously suggested explanation for the increased steady-state activity of R177A APE1 compared to that of WT APE1 (21). Substitution R181A has also been found to significantly facilitate product dissociation, but in addition, this substitution reduces the catalytic-step rate constant. It is worth pointing out that according to our results and other studies (22, 59), substitutions R177A and R181A have a significant effect on enzyme–product dissociation but a relatively weak impact on enzyme–substrate affinity. This fact confirms that the key function of these residues is facilitation of the enzyme–product binding, not the enabling of a rapid release of a cytotoxic DNA repair intermediate within a live cell. On the other hand, R181A has also been reported to considerably reduce the catalytic rate constant, suggesting that the previously observed (22) conformational change of Arg181 during the AP endonuclease reaction facilitates the chemical step of the APE1 enzyme–substrate interaction. Indeed, according to enzyme–substrate and enzyme–product crystal structures, Arg181 forms a hydrogen bond with Glu154 in the enzyme–substrate complex, but in the enzyme–product complex, Arg181 is shifted by 5.5 Å to come within hydrogen-bonding distance of the backbone phosphate upstream (5′) of the AP-site (22). Consequently, it can be proposed that Arg181's forming a hydrogen bond with the DNA phosphate may facilitate the positioning of the DNA backbone for cleavage. Alternatively, the impact of substitution R181A on the catalytic rate constant can be explained by the supposition that hydrogen bonding of Arg181 with Glu154 can give APE1 a more suitable conformation for the chemical-step execution.

Our assay of NIR and Exo-activities of mutants R177A and R181A revealed that these substitutions slightly decrease the activity toward the DHU- and αA-substrates and appreciably weaken the exonuclease activity. Therefore, we can conclude that Arg177 and Arg181 take part in APE1 exonuclease activity, but their participation is not critical because the mutants retain a quite effective exonuclease activity. The decreased exonuclease activity of R177A corroborates the recently proposed "RM bridge" consisting of Arg177 and Met270 playing a functional role in the exonuclease reaction (36). Nevertheless, the role of this interaction is not supported by kinetic data. Substitutions of each of the two amino acid residues forming the "RM bridge," Arg177 and Met270, have different effects on APE1 exonuclease activity: M270A barely affects APE1 exonuclease activity (30), whereas R177A decreases it significantly (present study). Furthermore, our and previous (30) data revealed that R177A and M270A substitutions have only a weak influence on APE1 substrate specificity, thus contradicting the proposed (36) key role of the "RM bridge" in APE1 substrate discrimination.

CONCLUSION

In this work, we clarified the functions of APE1 amino acid residues Tyr171, His309, Arg177, and Arg181 at different stages of the enzyme's catalytic mechanism and in APE1 substrate specificity. Taken together, our data indicate that substitutions Y171F and H309A weaken the chemical step of the AP endonuclease reaction by several orders of magnitude with retention of the F-site-containing-DNA–binding ability and without alterations of the pH dependence profile of the AP endonuclease activity. Substitutions R177A and R181A significantly facilitate the product dissociation stage while only weakly affecting DNA-binding efficiency, and in this context, R177A does not influence the chemical step, but R181A slows it severalfold due to a loss of the contact with the phosphate group. In addition, we demonstrated that substitutions R177A and R181A decrease the APE1 exonuclease activity noticeably, but overall, these substitutions were found to not affect APE1 substrate specificity strongly.

Author contributions

Conceptualization, N.A.K.; methodology, N.A.K. and O.S.F.; software, N.A.K. and O.S.F.; validation, A.S.B., N.A.K. and O.S.F.; formal analysis, A.S.B., A.A.K. and S.I.S.; investigation, A.S.B.; resources, A.A.I., M.S., N.A.K. and O.S.F.; data curation, A.S.B., N.A.K. and O.S.F.; writing—original draft preparation, N.A.K., A.A.I., M.S. and O.S.F.; writing—review and editing, N.A.K.; visualization, A.S.B. and N.A.K.; supervision, N.A.K.; project administration, N.A.K. and O.S.F.; funding acquisition, N.A.K., A.A.I., M.S. and O.S.F.

REFERENCES

1. Li, M., and Wilson 3rd, D. M. (2014) Human apurinic/apyrimidinic endonuclease 1. *Antioxid Redox Signal*. **20**, 678–707
2. Demple, B., and Sung, J.-S. (2005) Molecular and biological roles of Ape1 protein in mammalian base excision repair. *DNA Repair*. **4**, 1442–1449
3. Fung, H., and Demple, B. (2005) A vital role for Ape1/Ref1 protein in repairing spontaneous DNA damage in human cells. *Mol. Cell*. **17**, 463–470
4. Izumi, T., Brown, D. B., Naidu, C. V., Bhakat, K. K., MacInnes, M. A., Saito, H., Chen, D. J., and Mitra, S. (2005) Two essential but distinct functions of the mammalian abasic endonuclease. *Proc. Natl. Acad. Sci. U. S. A.* **102**, 5739–5743
5. Dyrkheeva, N. S., Lebedeva, N. A., and Lavrik, O. I. (2016) AP endonuclease 1 as a key enzyme in repair of apurinic/apyrimidinic sites. *Biochem.* **81**, 951–967
6. Evans, A. R., Limp-Foster, M., and Kelley, M. R. (2000) Going APE over ref-1. *Mutat Res*. **461**, 83–108
7. Dyrkheeva, N. S., Khodyreva, S. N., and Lavrik, O. I. (2007) Multifunctional human apurinic/apyrimidinic endonuclease 1: Role of additional functions. *Mol. Biol.* **41**, 402–416
8. Tell, G., Quadrifoglio, F., Tiribelli, C., and Kelley, M. R. (2009) The many functions of APE1/Ref-1: Not only a DNA repair enzyme. *Antioxidants Redox Signal.* 10.1089/ars.2008.2194
9. Wilson III, D. M., and Barsky, D. (2001) The major human abasic endonuclease: formation, consequences and repair of abasic lesions in DNA. *Mutat. Res.* **485**, 283–307
10. Gros, L., Ishchenko, A. A., Ide, H., Elder, R. H., and Saparbaev, M. K. (2004) The major human AP endonuclease (Ape1) is involved in the nucleotide incision repair pathway. *Nucleic Acids Res.* **32**, 73–81
11. Prorok, P., Alili, D., Saint-Pierre, C., Gasparutto, D., Zharkov, D. O., Ishchenko, A. A., Tudek, B., and Saparbaev, M. K. (2013) Uracil in duplex DNA is a substrate for the nucleotide incision repair pathway in human cells. *Proc. Natl. Acad. Sci. U S A.* **110**, E3695–E3703
12. Chou, K. M., and Cheng, Y. C. (2003) The exonuclease activity of human apurinic/apyrimidinic endonuclease (APE1). Biochemical properties and inhibition by the natural dinucleotide Gp4G. *J. Biol. Chem.* **278**, 18289–18296
13. Kuznetsova, A. A., Fedorova, O. S., and Kuznetsov, N. A. (2018) Kinetic Features of 3'-5' Exonuclease Activity of Human AP-Endonuclease APE1. *Molecules*. **23**, 2101
14. Dyrkheeva, N. S., Lomzov, A. A., Pyshnyi, D. V., Khodyreva, S. N., and Lavrik, O. I. (2006) Efficiency of exonucleolytic action of apurinic/apyrimidinic endonuclease 1 towards matched and mismatched dNMP at the 3′ terminus of different oligomeric DNA structures correlates with thermal stability of DNA duplexes. *Biochim. Biophys. Acta - Proteins Proteomics*. **1764**, 699–706
15. Chen, D. S., Herman, T., and Demple, B. (1991) Two distinct human DNA diesterases that hydrolyze 3′-blocking deoxyribose fragments from oxidized DNA. *Nucleic Acids Res.* **19**, 5907–5914
16. Barzilay, G., Walker, L. J., Robson, C. N., and Hickson, I. D. (1995) Site-directed mutagenesis of the human DNA repair enzyme HAP1: Identification of residues important for AP endonuclease and RNase H activity. *Nucleic Acids Res.* **23**, 1544–1550
17. Berquist, B. R., McNeill, D. R., and Wilson 3rd, D. M. (2008) Characterization of abasic endonuclease activity of human Ape1 on alternative substrates, as well as effects of ATP and sequence context on AP site incision. *J Mol Biol*. **379**, 17–27
18. Barnes, T., Kim, W. C., Mantha, A. K., Kim, S. E., Izumi, T., Mitra, S., and Lee, C. H. (2009) Identification of Apurinic/apyrimidinic endonuclease 1 (APE1) as the endoribonuclease that cleaves c-myc mRNA. *Nucleic Acids Res.* **37**, 3946–3958
19. Davletgildeeva, A. T., Kuznetsova, A. A., Fedorova, O. S., and Kuznetsov, N. A. (2020) Activity of Human Apurinic/Apyrimidinic Endonuclease APE1 Toward Damaged DNA and Native RNA With Non-canonical Structures. *Front. cell Dev. Biol.* **8**, 590848
20. Malfatti, M. C., Balachander, S., Antoniali, G., Koh, K. D., Saint-Pierre, C., Gasparutto, D., Chon, H., Crouch, R. J., Storici, F., and Tell, G. (2017) Abasic and oxidized ribonucleotides embedded in DNA are processed by human APE1 and not by RNase H2. *Nucleic Acids Res.* **45**, 11193–11212

21. Mol, C. D., Izumi, T., Mitra, S., and Tainer, J. A. (2000) DNA-bound structures and mutants reveal abasic DNA binding by APE1 and DNA repair coordination. *Nature*. **403**, 451–456
22. Freudenthal, B. D., Beard, W. A., Cuneo, M. J., Dyrkheeva, N. S., and Wilson, S. H. (2015) Capturing snapshots of APE1 processing DNA damage. *Nat Struct Mol Biol*. **22**, 924–931
23. Whitaker, A. M., Flynn, T. S., and Freudenthal, B. D. (2018) Molecular snapshots of APE1 proofreading mismatches and removing DNA damage. *Nat. Commun.* **9**, 399
24. Manvilla, B. A., Pozharski, E., Toth, E. A., and Drohat, A. C. (2013) Structure of human apurinic/apyrimidinic endonuclease 1 with the essential Mg2+ cofactor. *Acta Crystallogr. D Biol. Crystallogr*. **69**, 2555–2562
25. He, H., Chen, Q., and Georgiadis, M. M. (2014) High-resolution crystal structures reveal plasticity in the metal binding site of apurinic/apyrimidinic endonuclease I. *Biochemistry*. **53**, 6520–9
26. Lipton, A. S., Heck, R. W., Primak, S., McNeill, D. R., Wilson 3rd, D. M., and Ellis, P. D. (2008) Characterization of Mg2+ binding to the DNA repair protein apurinic/apyrimidic endonuclease 1 via solid-state 25Mg NMR spectroscopy. *J Am Chem Soc*. **130**, 9332–9341
27. Gattuso, H., Durand, E., Bignon, E., Morell, C., Georgakilas, A. G., Dumont, E., Chipot, C., Dehez, F., and Monari, A. (2016) Repair Rate of Clustered Abasic DNA Lesions by Human Endonuclease: Molecular Bases of Sequence Specificity. *J. Phys. Chem. Lett.* 10.1021/acs.jpclett.6b01692
28. Kuznetsova, A. A., Matveeva, A. G., Milov, A. D., Vorobjev, Y. N., Dzuba, S. A., Fedorova, O. S., and Kuznetsov, N. A. (2018) Substrate specificity of human apurinic/apyrimidinic endonuclease APE1 in the nucleotide incision repair pathway. *Nucleic Acids Res.* **46**, 11454–11465
29. Bulygin, A. A., Kuznetsova, A. A., Vorobjev, Y. N., Fedorova, O. S., and Kuznetsov, N. A. (2020) The Role of Active-Site Plasticity in Damaged-Nucleotide Recognition by Human Apurinic/Apyrimidinic Endonuclease APE1. *Molecules*. 10.3390/molecules25173940
30. Alekseeva, I. V., Kuznetsova, A. A., Bakman, A. S., Fedorova, O. S., and Kuznetsov, N. A. (2020) The role of active-site amino acid residues in the cleavage of DNA and RNA substrates by human apurinic/apyrimidinic endonuclease APE1. *BBA - Gen. Subj.* 10.1016/j.bbagen.2020.129718
31. Aboelnga, M. M., and Wetmore, S. D. (2019) Unveiling a Single-Metal-Mediated Phosphodiester Bond Cleavage Mechanism for Nucleic Acids: A Multiscale Computational Investigation of a Human DNA Repair Enzyme. *J. Am. Chem. Soc.* **141**, 8646–8656
32. Mundle, S. T., Fattal, M. H., Melo, L. F., Coriolan, J. D., O'Regan, N. E., and Strauss, P. R. (2004) Novel role of tyrosine in catalysis by human AP endonuclease 1. *DNA Repair (Amst).* **3**, 1447–1455
33. Alekseeva, I. V., Bakman, A. S., Vorobjev, Y. N., Fedorova, O. S., and Kuznetsov, N. A. (2019) Role of Ionizing Amino Acid Residues in the Process of DNA Binding by Human AP Endonuclease 1 and in Its Catalysis. *J. Phys. Chem. B.* **123**, 9546–9556
34. Gorman, M. A., Morera, S., Rothwell, D. G., de La Fortelle, E., Mol, C. D., Tainer, J. A., Hickson, I. D., and Freemont, P. S. (1997) The crystal structure of the human DNA repair endonuclease HAP1 suggests the recognition of extra-helical deoxyribose at DNA abasic sites. *EMBO J.* **16**, 6548–6558
35. Mundle, S. T., Delaney, J. C., Essigmann, J. M., and Strauss, P. R. (2009) Enzymatic mechanism of human apurinic/apyrimidinic endonuclease against a THF AP site model substrate. *Biochemistry*. **48**, 19–26
36. Liu, T. C., Lin, C. T., Chang, K. C., Guo, K. W., Wang, S., Chu, J. W., and Hsiao, Y. Y. (2021) APE1 distinguishes DNA substrates in exonucleolytic cleavage by induced space-filling. *Nat. Commun.* 10.1038/s41467-020-20853-2
37. Whitaker, A. M., and Freudenthal, B. D. (2018) APE1: A skilled nucleic acid surgeon. *DNA Repair (Amst).* **71**, 93–100
38. Hoitsma, N. M., Whitaker, A. M., Beckwitt, E. C., Jang, S., Agarwal, P. K., Van Houten, B., and Freudenthal, B. D. (2020) AP-endonuclease 1 sculpts DNA through an anchoring tyrosine residue on the DNA intercalating loop. *Nucleic Acids Res.* **48**, 7345–7355
39. Timofeyeva, N. A., Koval, V. V, Knorre, D. G., Zharkov, D. O., Saparbaev, M. K., Ishchenko, A.

A., and Fedorova, O. S. (2009) Conformational dynamics of human AP endonuclease in base excision and nucleotide incision repair pathways. *J. Biomol. Struct. Dyn.* **26**, 637–652
40. Kanazhevskaya, L. Y., Koval, V. V, Zharkov, D. O., Strauss, P. R., and Fedorova, O. S. (2010) Conformational transitions in human AP endonuclease 1 and its active site mutant during abasic site repair. *Biochemistry*. **49**, 6451–6461
41. Alekseeva, I. V., Davletgildeeva, A. T., Arkova, O. V., Kuznetsov, N. A., and Fedorova, O. S. (2019) The impact of single-nucleotide polymorphisms of human apurinic/apyrimidinic endonuclease 1 on specific DNA binding and catalysis. *Biochimie*. **163**, 73–83
42. Kanazhevskaya, L. Y., Koval, V. V, Vorobjev, Y. N., and Fedorova, O. S. (2012) Conformational dynamics of abasic DNA upon interactions with AP endonuclease 1 revealed by stopped-flow fluorescence analysis. *Biochemistry*. **51**, 1306–1321
43. Miroshnikova, A. D., Kuznetsova, A. A., Vorobjev, Y. N., Kuznetsov, N. A., and Fedorova, O. S. (2016) Effects of mono- and divalent metal ions on DNA binding and catalysis of human apurinic/apyrimidinic endonuclease 1. *Mol. BioSyst.* **12**, 1527–1539
44. Miroshnikova, A. D., Kuznetsova, A. A., Kuznetsov, N. A., and Fedorova, O. S. (2016) Thermodynamics of Damaged DNA Binding and Catalysis by Human AP Endonuclease 1. *Acta Naturae*. **8**, 103–110
45. Kuznetsova, A. A., Kuznetsov, N. A., Ishchenko, A. A., Saparbaev, M. K., and Fedorova, O. S. (2014) Pre-steady-state fluorescence analysis of damaged DNA transfer from human DNA glycosylases to AP endonuclease APE1. *Biochim. Biophys. Acta*. **1840**, 3042–3051
46. Yakovlev, D. A., Kuznetsova, A. A., Fedorova, O. S., and Kuznetsov, N. A. (2017) Search for Modified DNA Sites with the Human Methyl-CpG-Binding Enzyme MBD4. *Acta Naturae*. **9**, 88–98
47. Kuznetsova, A. A., Iakovlev, D. A., Misovets, I. V., Ishchenko, A. A., Saparbaev, M. K., Kuznetsov, N. A., and Fedorova, O. S. (2017) Pre-steady-state kinetic analysis of damage recognition by human single-strand selective monofunctional uracil-DNA glycosylase SMUG1. *Mol Biosyst*. **13**, 2638–2649
48. Kladova, O. A., Kuznetsova, A. A., Fedorova, O. S., and Kuznetsov, N. A. (2017) Mutational and Kinetic Analysis of Lesion Recognition by Escherichia coli Endonuclease VIII. *Genes (Basel)*. **8**, 1–13
49. Kuzmic, P. (1996) Program DYNAFIT for the analysis of enzyme kinetic data: application to HIV proteinase. *Anal. Biochem.* **237**, 260–273
50. Kladova, O. A., Krasnoperov, L. N., Kuznetsov, N. A., and Fedorova, O. S. (2018) Kinetics and thermodynamics of DNA processing by wild type DNA-glycosylase endo III and its catalytically inactive mutant forms. *Genes (Basel).* 10.3390/genes9040190
51. Kuznetsov, N. A., Kuznetsova, A. A., Vorobjev, Y. N., Krasnoperov, L. N., and Fedorova, O. S. (2014) Thermodynamics of the DNA damage repair steps of human 8-oxoguanine DNA glycosylase. *PLoS One*. **9**, e98495
52. Kuznetsov, N. A., Vorobjev, Y. N., Krasnoperov, L. N., and Fedorova, O. S. (2012) Thermodynamics of the multi-stage DNA lesion recognition and repair by Formamidopyrimidine-DNA glycosylase using pyrrolocytosine fluorescence - Stopped-flow pre-steady-state kinetics. *Nucleic Acids Res.* **40**, 7384–7392
53. Kuznetsov, N. A., Koval, V. V., Zharkov, D. O., and Fedorova, O. S. (2012) Conformational dynamics of the interaction of Escherichia coli endonuclease VIII with DNA substrates. *DNA Repair*. **11**, 884–891
54. Straume, M., and Johnson, M. L. (1992) Monte Carlo Method for determining complete confidence probability distributions of estimated model parameters. *Methods Enzymol.* **210**, 117–129
55. Tsutakawa, S. E., Shin, D. S., Mol, C. D., Izumi, T., Arvai, A. S., Mantha, A. K., Szczesny, B., Ivanov, I. N., Hosfield, D. J., Maiti, B., Pique, M. E., Frankel, K. A., Hitomi, K., Cunningham, R. P., Mitra, S., and Tainer, J. A. (2013) Conserved structural chemistry for incision activity in structurally non-homologous apurinic/apyrimidinic endonuclease APE1 and endonuclease IV DNA repair enzymes. *J. Biol. Chem.* **288**, 8445–8455

56. Maher, R. L., and Bloom, L. B. (2007) Pre-steady-state kinetic characterization of the AP endonuclease activity of human AP endonuclease 1. *J Biol Chem*. **282**, 30577–30585
57. Erzberger, J. P., and Wilson 3rd, D. M. (1999) The role of Mg2+ and specific amino acid residues in the catalytic reaction of the major human abasic endonuclease: new insights from EDTA-resistant incision of acyclic abasic site analogs and site-directed mutagenesis. *J Mol Biol*. **290**, 447–457
58. Kim, W.-C., Berquist, B. R., Chohan, M., Uy, C., Wilson, D. M., and Lee, C. H. (2011) Characterization of the endoribonuclease active site of human apurinic/apyrimidinic endonuclease 1. *J. Mol. Biol.* **411**, 960–71
59. Peddi, S. R., Chattopadhyay, R., Naidu, C. V., and Izumi, T. (2006) The human apurinic/apyrimidinic endonuclease-1 suppresses activation of poly(adp-ribose) polymerase-1 induced by DNA single strand breaks. *Toxicology*. **224**, 44–55
60. Kuznetsov, N. A., Kupryushkin, M. S., Abramova, T. V., Kuznetsova, A. A., Miroshnikova, A. D., Stetsenko, D. A., Pyshnyi, D. V., and Fedorova, O. S. (2015) New oligonucleotide derivatives as unreactive substrate analogues and potential inhibitors of human apurinic/apyrimidinic endonuclease APE1. *Mol Biosyst*. **12**, 67–75
61. Wong, D., DeMott, M. S., and Demple, B. (2003) Modulation of the 3′→5′-exonuclease activity of human apurinic endonuclease (Ape1) by its 5′-incised abasic DNA product. *J. Biol. Chem.* **278**, 36242–36249

FOOTNOTES

* This work was supported partially by a Russian-Government–funded project (No. 121031300041-4), by Electricité de France (RB 2021-05, to M.S) and by French National Research Agency (ANR-18-CE44-0008, to A.A.I.). The part of this work involving Trp detection combined with stopped-flow kinetics was specifically funded by Russian Science Foundation grant No. 21-64-00017.

SCHEMES AND FIGURES LEGENDS

Scheme 1. Enzyme deprotonation process.

Scheme 2. The kinetic mechanism of APE1 Y171F and H309A binding to the F-site–containing DNA substrates revealed by Trp fluorescence or FRET fluorescence intensity detection. E is the enzyme, S is the DNA substrate, ES is the enzyme–substrate complex; $k_1/k_{-1} = K_S$: the thermodynamic constant of enzyme–substrate association.

Scheme 3. The kinetic mechanism underlying the processing of the F-substrate by WT, R177A, and R181A APE1, as revealed by Trp fluorescence or FRET fluorescence intensity detection. E represents the enzyme, S is the F-site–containing DNA substrate, P denotes the DNA product, ES is the enzyme–substrate complex, and EP stands for the enzyme–product complex; $k_3/k_{-3} = K_P$: the product dissociation thermodynamic constant. In some cases, we could not determine constants k_3 and k_{-3} separately but could determine their ratio, K_P.

FIGURE 1. Focused view of the APE1 active site with the most important for catalysis amino acid residues (shown in green) and with the THF phosphorothioate DNA substrate (shown in tan) in the crystal structure of enzyme-substrate complex (PDB ID 5DG0). The potential hydrogen bonds are shown by dashes with distances in angstroms. A probable nucleophilic water molecule is shown with the inline attack shown with a red arrow. The distance (Å) between this supposed nucleophilic water and phosphate group is indicated. It can be seen that in this structure the residues Tyr171 and His309 can form hydrogen bonds with scissile phosphate when being protonated. While, the Asp210 can activate the nucleophilic water molecule (A). The hypothetical model of APE1 DNA cleavage mechanism derived from APE1 bound to DNA crystal structures (22). In this model Asp210 being deprotonated activates a nucleophilic water molecule and Tyr171 and His309 being protonated coordinate scissile phosphate stabilizing the reaction transition state (B). The alternative hypothetical model of APE1 DNA cleavage mechanism in which deprotonated His309 activates a nucleophilic water molecule (34, 35) (C).

FIGURE 2. Structural alignment of the APE1 exonuclease–substrate complex with a C/T mismatch (Protein Data Bank [PDB] ID 5WN4) and APE1 endonuclease–substrate complex with F-site–containing DNA (PDB ID 1DE8). In the structure of the exonuclease complex, the protein is yellow, the DNA is tan, and the mismatched C that is excised by APE1 via its exonuclease action is colored golden. In the structure of the endonuclease complex, the protein is green, the DNA is green, and the F-site is olive-green. Readers can see that the F-site is flipped into the APE1 active site while the mismatched 3′ cytosine is placed within the intrahelical DNA cavity without nucleotide flipping.

FIGURE 3. X-ray structure of APE1 complexed with DNA containing an F-site (PDB ID 1DE8). Residues Tyr171, His309, Arg177, and Arg181 are blue, and the F-site residue [(2*R*,3*S*)-2-(hydroxymethyl)-3-hydroxytetrahydrofuran] is black.

FIGURE 4. F-site cleavage activity of WT APE1 and its mutants as detected by PAGE product accumulation analysis. [Enzyme] = 0.05 μM, [DNA substrate] = 1.0 μM, the reaction time was 10 s.

FIGURE 5. Kinetic time courses of single-turnover product accumulation for APE1 mutants H309A (A) and Y171F (B). Kinetic curves are fitted to Eq. 1. [Enzyme] = 1.0 μM, [DNA substrate] = 1.0 μM.

FIGURE 6. The impact of pH on the activity of mutants Y171F (A) and H309A (B). These dependences were fitted to Eq. 6 to obtain pK_a values. [Enzyme] = 1.0 μM, [DNA substrate] = 1.0 μM, the reaction time was 10 min for Y171F and 30 min for H309A.

FIGURE 7. Changes in FAM fluorescence intensity during the interaction of WT (A), Y171F (B), H309A (C), R177A (D), or R181A (E) APE1 with the FRET-F-substrate. Concentrations of the enzymes and FRET-F-substrate (schematically depicted in panel A) are indicated in the panels. Experimental data and results of global fitting are presented as jagged and smooth traces, respectively.

FIGURE 8. Changes in Trp fluorescence intensity during the interaction of WT (A), Y171F (B), H309A (C), R177A (D), or R181A (E) APE1 with the F/G-substrate. Concentrations of the enzymes and F/G-substrate (schematically depicted in panel A) are indicated in the panels. Experimental data and results of global fitting are presented as jagged and smooth traces, respectively.

FIGURE 9. DHU (A) and αA (B) DNA cleavage activity of WT APE1 and its mutants as detected by PAGE product accumulation analysis. [Enzyme] = 2.0 μM, [DNA substrate] = 1.0 μM, the reaction time was 5 min for DHU and 2 hours for αA.

FIGURE 10. Exonuclease activity of WT APE1 and its mutants as detected by PAGE product accumulation analysis. [Enzyme] = 2.0 μM, [DNA substrate] = 1.0 μM, the reaction time points were 1 and 5 min (noted in the figure)).

TABLES

Table 1. Sequences of ODNs.[a]

Shorthand	Sequence
F/G	5'-GCTCA**F**GTACAGAGCTG-3' 3'-CGAGT**G**CATGTCTCGAC-5'
FAM-F/G	5'-**FAM**-GCTCA**F**GTACAGAGCTG-3' 3'-CGAGT**G**CATGTCTCGAC-5'
FRET-F/G	5'-**FAM**-GCTCA**F**GTACAGAGCTG-3' 3'-CGAGT**G**CATGTCTCGAC-**BHQ1**-5'
FAM-DHU/G	5'-**FAM**-GCTCA(**DHU**)GTACAGAGCTG-3' 3'-CGAGT **G** CATGTCTCGAC-5'
FAM-αA/T	5'-**FAM**-GCTCA(**αA**)GTACAGAGCTG-3' 3'-CGAGT **T** CATGTCTCGAC-5'
Exo-substrate	5'-**FAM**-CAGCTCTGTACGTGAGC-3' 3'-GTCGAGACATGCACTCGTCACCACTGTG-5'

[a]FAM is 6-carboxyfluorescein, BHQ1 is black hole quencher, FRET is Förster resonance energy transfer, F is (2*R*,3*S*)-2-(hydroxymethyl)-3-hydroxytetrahydrofuran (a reduced abasic site analog), DHU is 5,6-dihydrouridine, and αA is the α-anomer of 2′-deoxyadenosine.

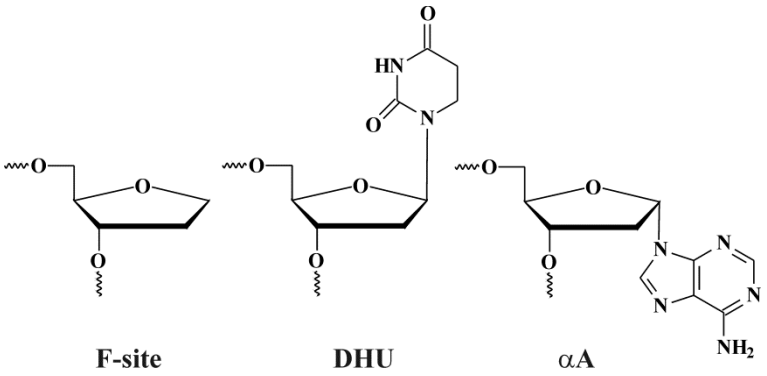

Table 2. Concentrations and reaction times for the PAGE assays of DNA cleavage.

Experiment	Reactant concentrations	Reaction time
Comparison of APE1 mutants' activities	[E] = 0.05 μM [S] = 1.0 μM	10 s
Kinetic time courses for mutants Y171F and H309A	[E] = 1.0 μM [S] = 1.0 μM	the reactions were quenched at multiple time points between minutes 1 and 180
pH-dependence assay for Y171F	[E] = 1.0 μM [S] = 1.0 μM	10 min
pH dependence assay for H309A	[E] = 1.0 μM [S] = 1.0 μM	30 min
NIR activity assay for DHU/G-substrate	[E] = 2.0 μM [S] = 1.0 μM	5 min
NIR activity assay for αA/T-substrate	[E] = 2.0 μM [S] = 1.0 μM	2 h
Exonuclease activity assay	[E] = 2.0 μM [S] = 1.0 μM	1 and 5 min

Table 3. Kinetic parameters of the interaction of WT and mutant forms APE1 with F-site containing substrate revealed by FRET fluorescence traces analysis.

	$k_1\times10^{-6}$, $M^{-1}s^{-1}$	k_{-1}, s^{-1}	$K_S\times10^{-6}$, M^{-1}	k_2, s^{-1}	k_3, s^{-1}	$k_{-3}\times10^{-6}$, $M^{-1}s^{-1}$	$K_P\times10^6$, M	v_i, μM/s
Y171F	230 ±20	140 ±20	1.6 ±0.4					
H309A	160 ±60	200 ±40	0.8 ±0.5					
WT	350 ±40	20 ±4	18 ±6	2.22 ±0.03	0.38 ±0.02	26 ±4	0.015 ±0.003	0.015 ±0.001
R177A	520 ± 10	75 ±7	7 ±1	2.36 ±0.02	8.0 ±0.3	1.6 ±0.2	5 ±1	0.080 ±0.006
R181A	740 ±90	110 ±40	7 ±3	0.73 ±0.03	1.4 ±0.2	18 ±7	0.08 ±0.04	0.021 ±0.006

$K_S = k_1/k_{-1}$, $K_P = k_3/k_{-3}$, $V_{max} = k_2k_3\times E_0/(k_2 + k_3)$, $v_i = V_{max}\times S/(K_S + S)$

Table 4. Kinetic parameters of the interaction of WT and mutant APE1 forms with the F-site–containing substrate as revealed by analysis of Trp fluorescence traces.

	$k_1 \times 10^{-6}$, $M^{-1}s^{-1}$	k_{-1}, s^{-1}	$K_S \times 10^{-6}$, M^{-1}	k_2, s^{-1}	$K_P \times 10^{6}$, M
Y171F	620 ±50	19 ±4	30 ±10		
H309A	430 ±30	50 ±10	9 ±2		
WT	1600 ±100	50 ±20	30 ±15	2.4 ±0.2	0.06 ±0.01
R177A	430 ±10	15 ±2	29 ±5	2.3 ±0.1	0.10 ±0.02
R181A	1170 ± 60	80 ±20	15 ±5	0.61 ±0.03	0.12 ±0.02

$K_S = k_1/k_{-1}$
$K_P = k_3/k_{-3}$

FIGURES

A

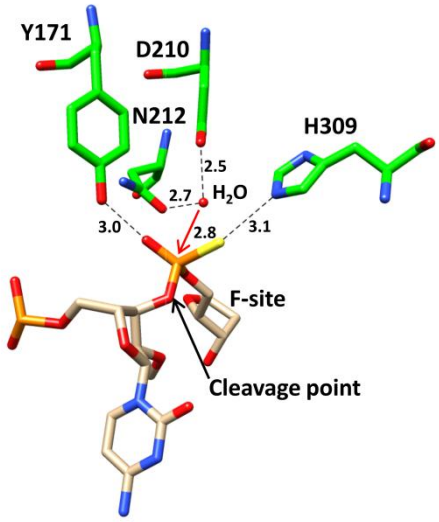

B

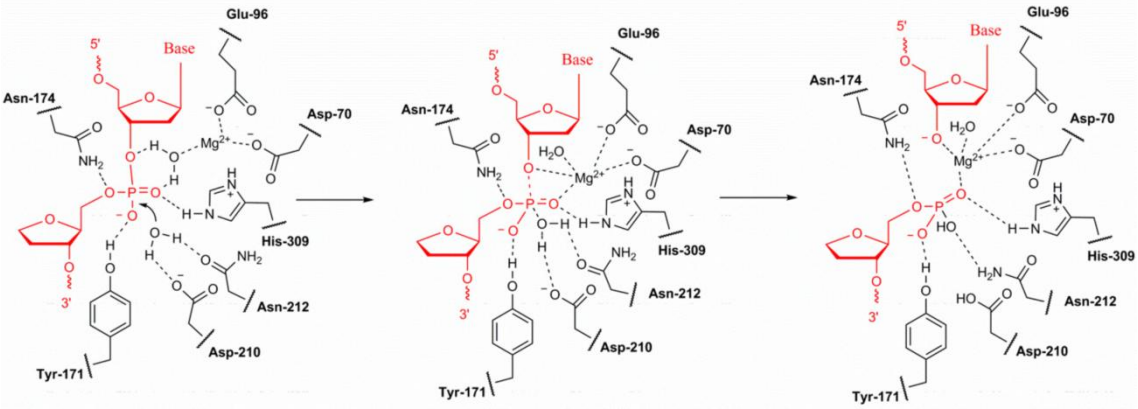

C

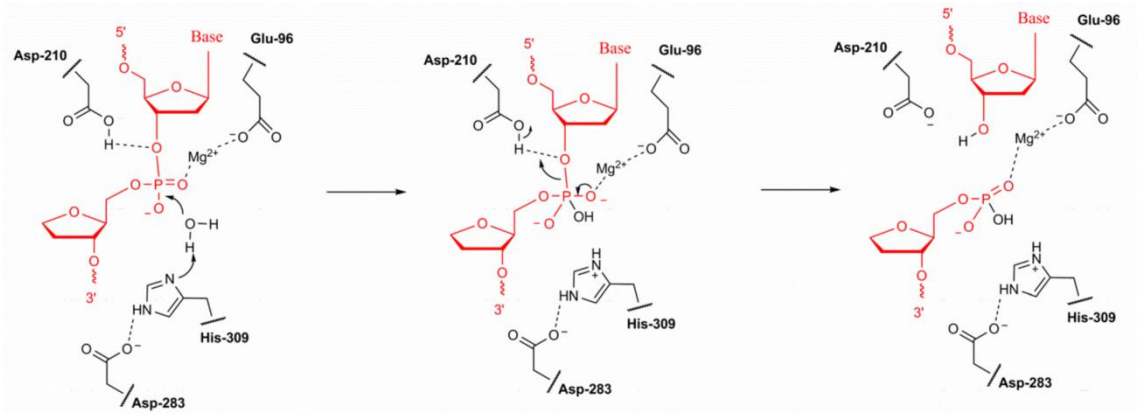

Figure 1

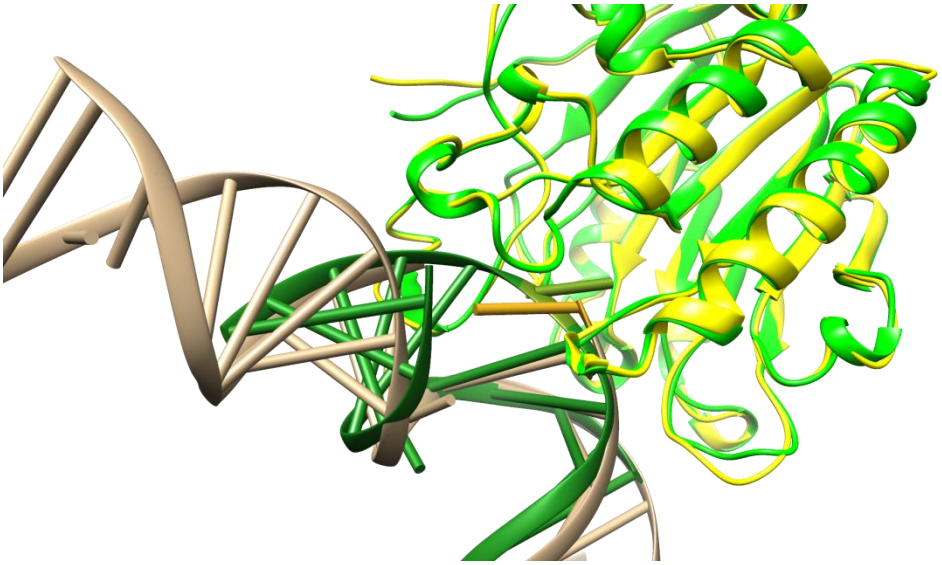

Figure 2

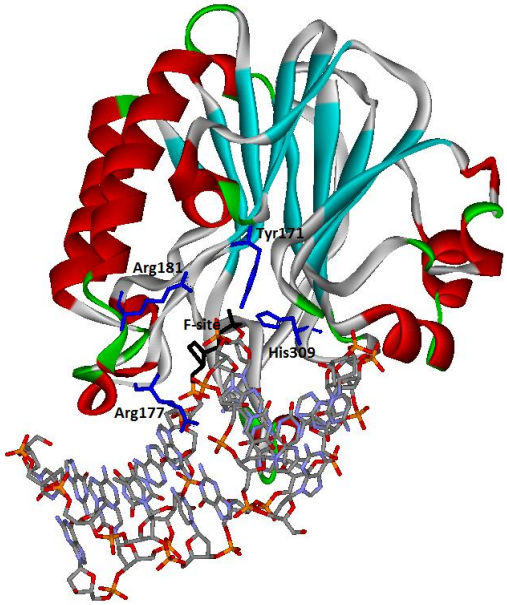

Figure 3

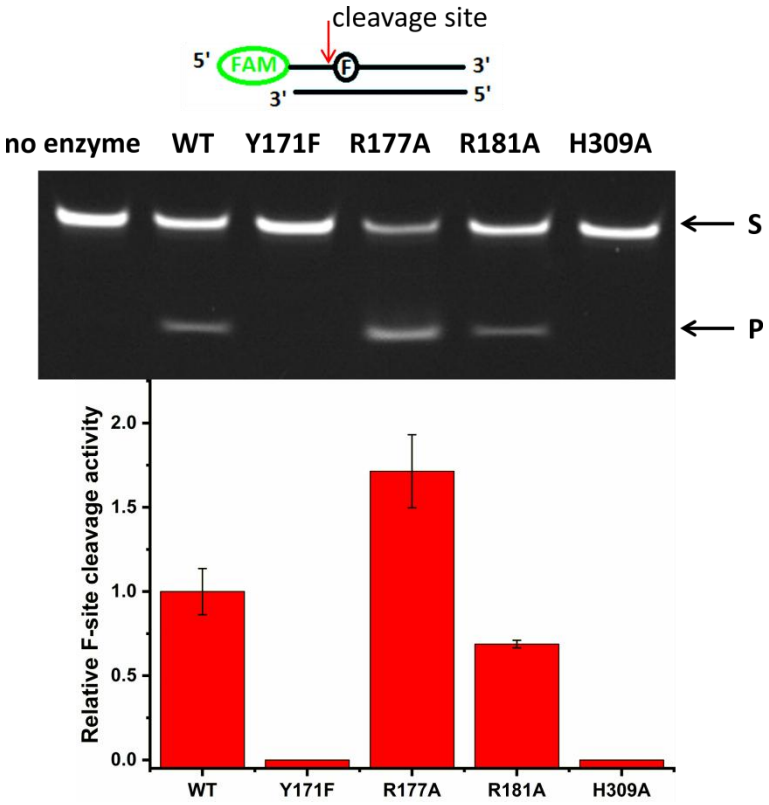
cleavage site
5'
FAM
F
3'
3'
5'
no enzyme
WT
Y171F
R177A
R181A
H309A
S
P
Relative F-site cleavage activity
2.0
1.5
1.0
0.5
0.0
WT
Y171F
R177A
R181A
H309A

Figure 4

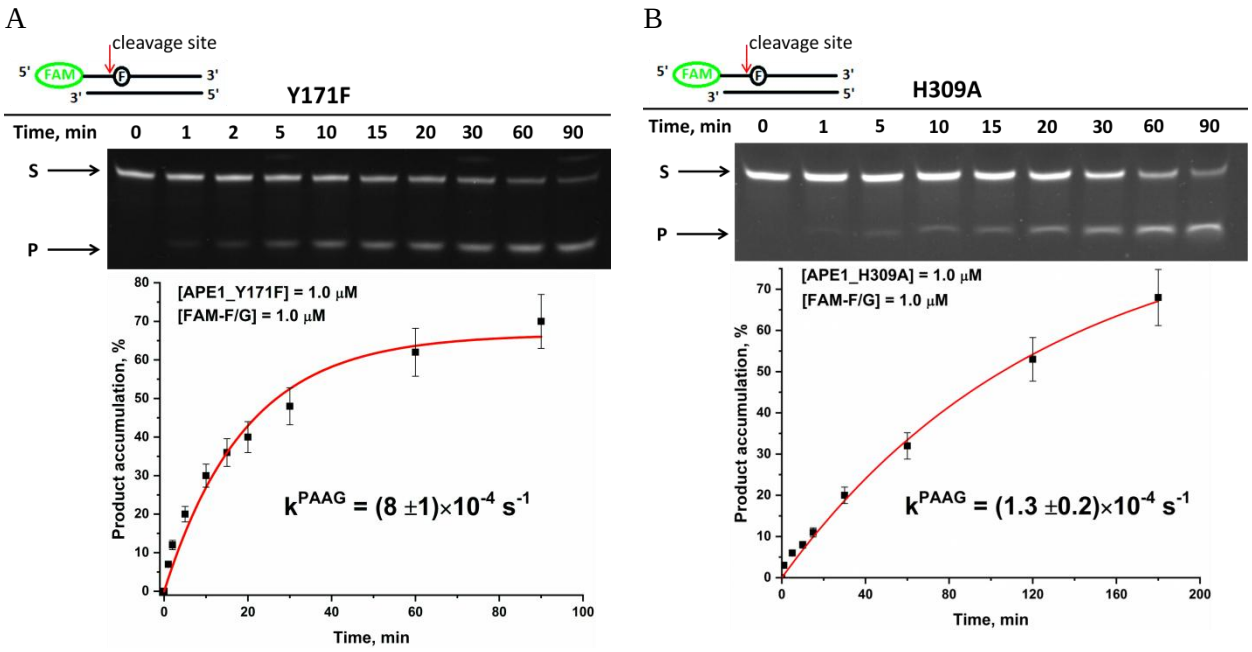
A
cleavage site
5'
FAM
F
3'
3'
5'
Y171F
Time, min
0
1
2
5
10
15
20
30
60
90
S
P
[APE1_Y171F] = 1.0 μM
[FAM-F/G] = 1.0 μM
Product accumulation, %
k^PAAG = (8 ±1)×10^-4 s^-1
Time, min
B
cleavage site
H309A
[APE1_H309A] = 1.0 μM
[FAM-F/G] = 1.0 μM
Product accumulation, %
k^PAAG = (1.3 ±0.2)×10^-4 s^-1
Time, min

Figure 5

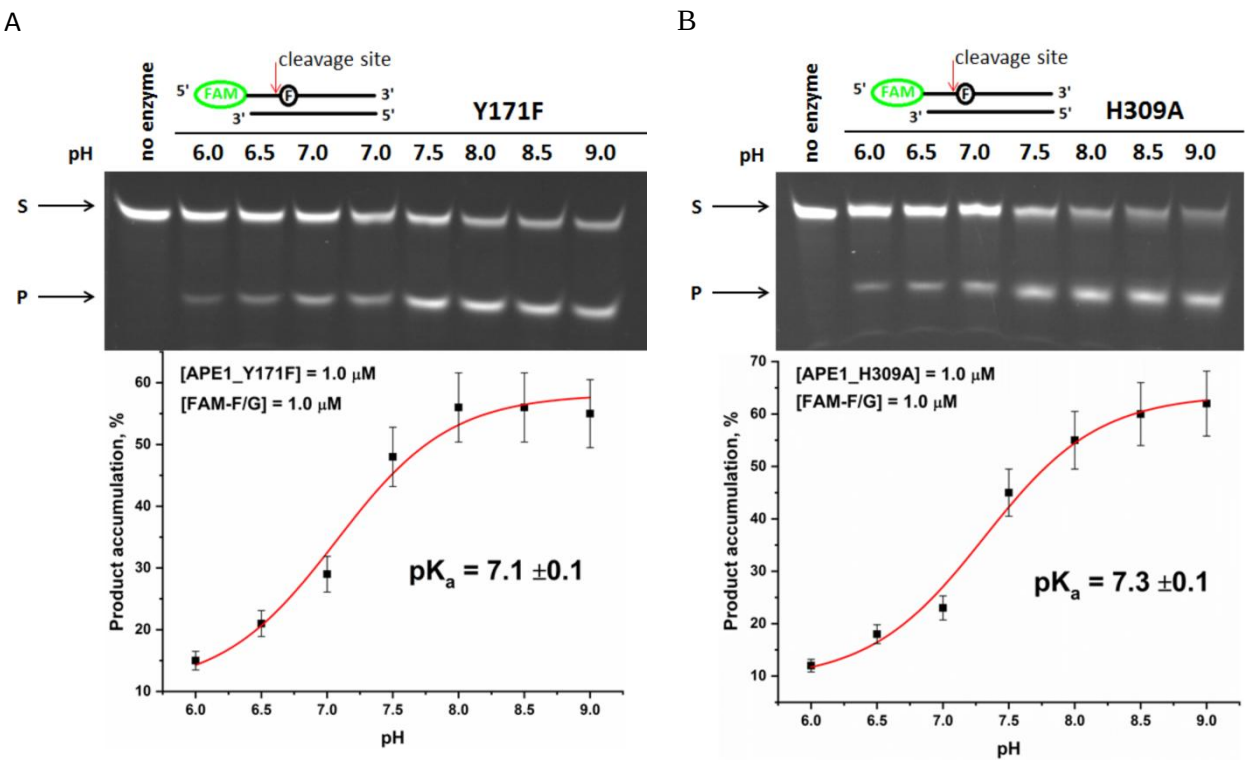
A
B
cleavage site
5'
FAM
F
3'
3'
5'
Y171F
H309A
no enzyme
pH
6.0 6.5 7.0 7.0 7.5 8.0 8.5 9.0
S
P
[APE1_Y171F] = 1.0 μM
[FAM-F/G] = 1.0 μM
[APE1_H309A] = 1.0 μM
[FAM-F/G] = 1.0 μM
Product accumulation, %
pK$_a$ = 7.1 ±0.1
pK$_a$ = 7.3 ±0.1
pH

Figure 6

A

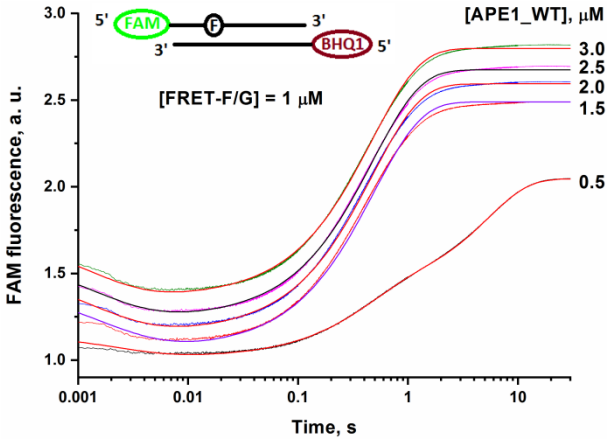

B

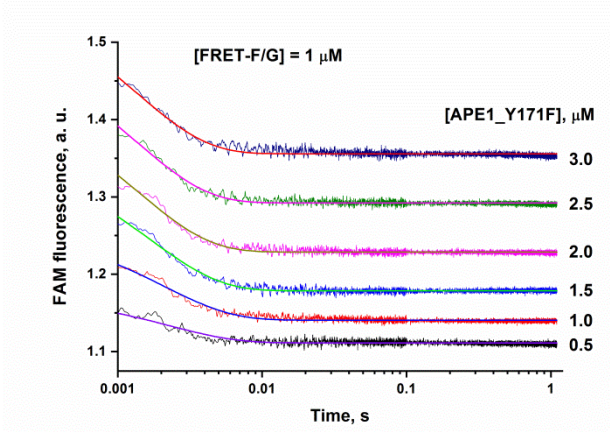

C

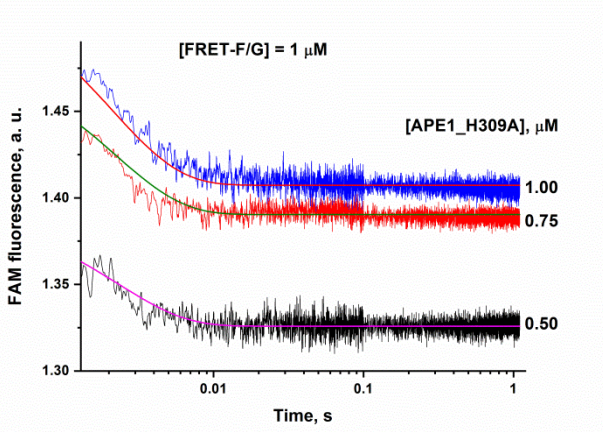

D

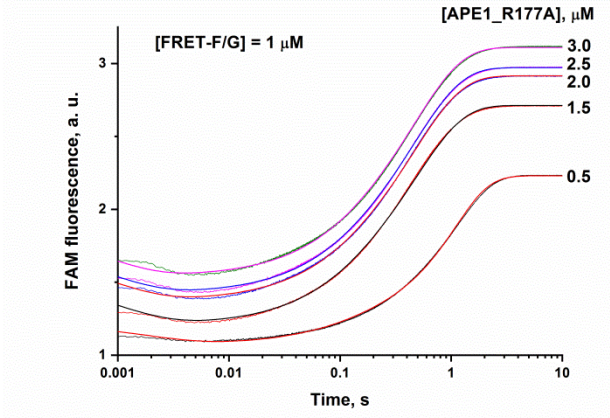

E

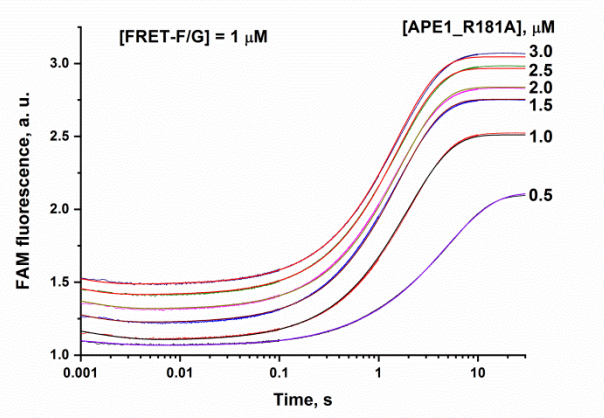

Figure 7

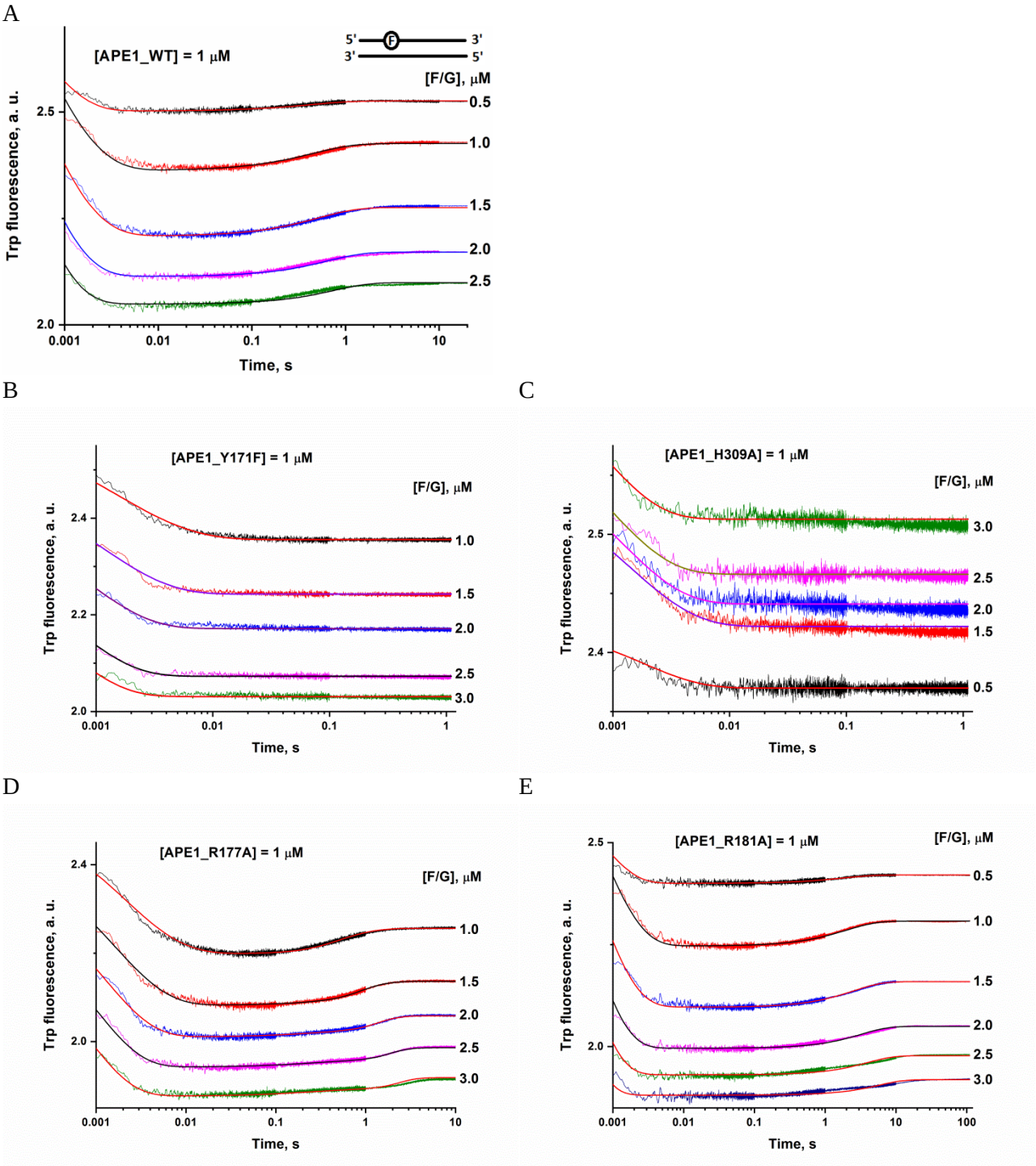
A
[APE1_WT] = 1 μM
5'
3'
F
3'
5'
[F/G], μM
0.5
1.0
1.5
2.0
2.5
Trp fluorescence, a. u.
Time, s
B
C
[APE1_Y171F] = 1 μM
[F/G], μM
1.0
1.5
2.0
2.5
3.0
Trp fluorescence, a. u.
Time, s
[APE1_H309A] = 1 μM
[F/G], μM
3.0
2.5
2.0
1.5
0.5
Trp fluorescence, a. u.
Time, s
D
E
[APE1_R177A] = 1 μM
[F/G], μM
1.0
1.5
2.0
2.5
3.0
Trp fluorescence, a. u.
Time, s
[APE1_R181A] = 1 μM
[F/G], μM
0.5
1.0
1.5
2.0
2.5
3.0
Trp fluorescence, a. u.
Time, s

Figure 8

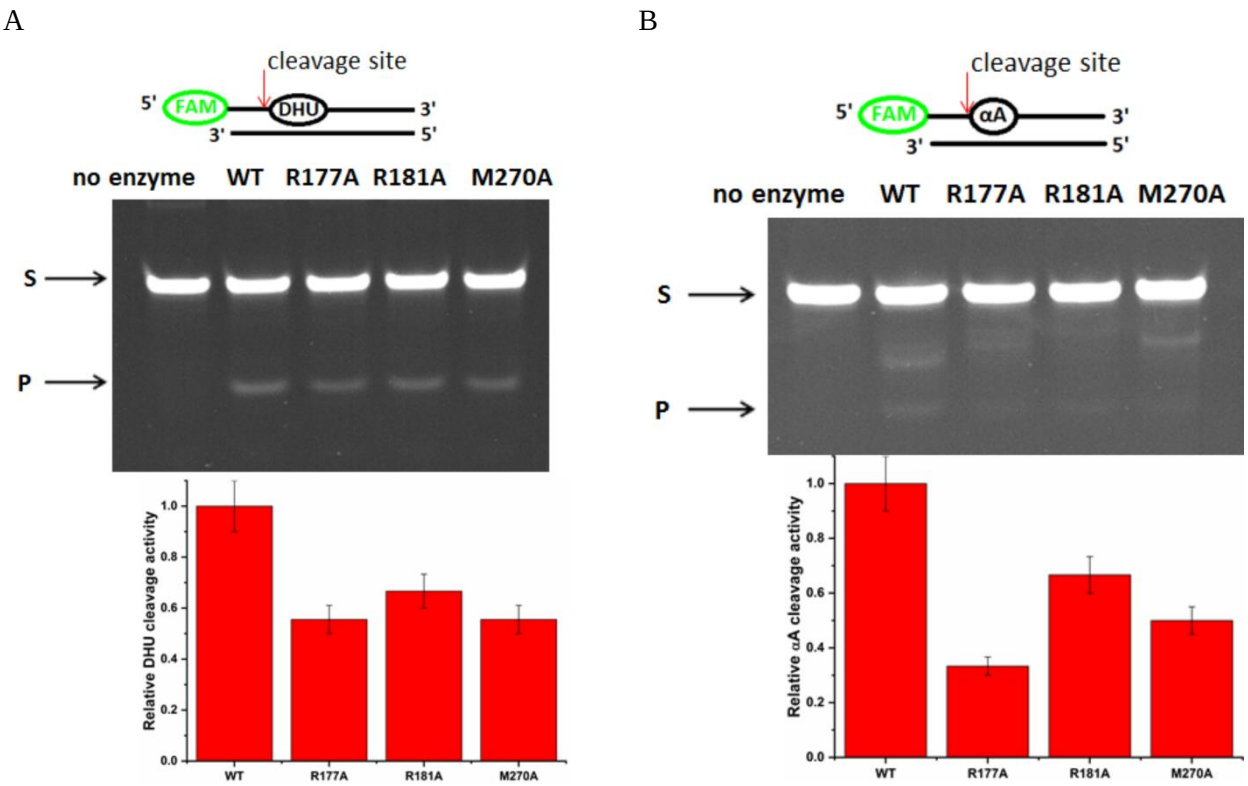
A
cleavage site
5'
FAM
DHU
3'
3'
5'
no enzyme
WT
R177A
R181A
M270A
S
P
Relative DHU cleavage activity
1.0
0.8
0.6
0.4
0.2
0.0
WT
R177A
R181A
M270A
B
cleavage site
5'
FAM
αA
3'
3'
5'
no enzyme
WT
R177A
R181A
M270A
S
P
Relative αA cleavage activity
1.0
0.8
0.6
0.4
0.2
0.0
WT
R177A
R181A
M270A

Figure 9

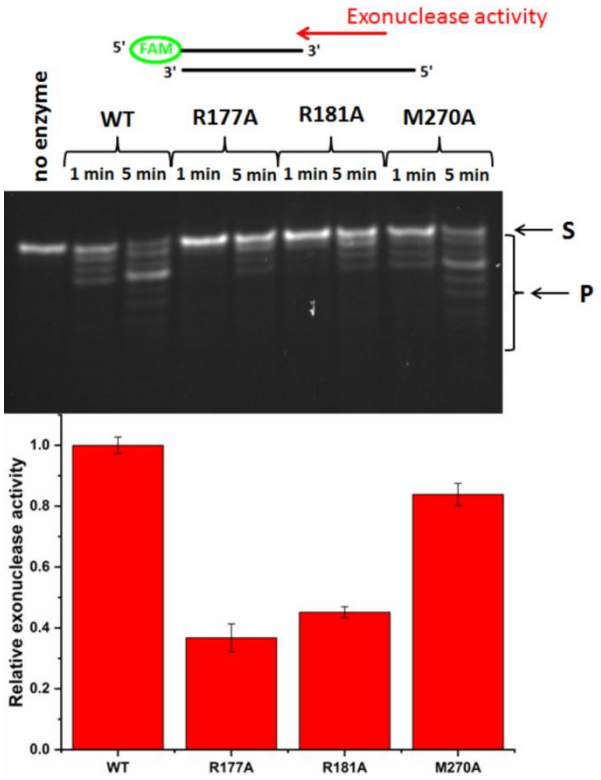
Exonuclease activity
5'
FAM
3'
3'
5'
no enzyme
WT
R177A
R181A
M270A
1 min 5 min 1 min 5 min 1 min 5 min 1 min 5 min
S
P
Relative exonuclease activity
1.0
0.8
0.6
0.4
0.2
0.0
WT
R177A
R181A
M270A

Figure 10